Nanotechnology **21** (2010) 045201 (6pp) doi:10.1088/0957-4484/21/4/045201

The effect of catalysts and underlayer metals on the properties of PECVD-grown carbon nanostructures

Xuhui Sun[1,3], Ke Li[2], Raymond Wu[2], Patrick Wilhite[2], Tsutomu Saito[2], Jing Gao[1] and Cary Y Yang[2]

[1] Functional Nano and Soft Materials Laboratory (FUNSOM), Soochow University, 199 Ren-Ai Road, Suzhou Industrial Park, Suzhou, Jiangsu 215123, People's Republic of China
[2] Center for Nanostructures, Santa Clara University, Santa Clara, CA 95053, USA

E-mail: xhsun@suda.edu.cn

Received 25 August 2009, in final form 18 November 2009
Published 10 December 2009
Online at stacks.iop.org/Nano/21/045201

Abstract
The growth behaviors and contact resistances of vertically aligned carbon nanotubes (CNTs) and carbon nanofibers (CNFs) grown on different underlayer metals are investigated. The average diameter, diameter distribution, density, growth rate and contact resistance exhibit strong correlation with the choice of catalyst/underlayer combination. These observations are analyzed in terms of interactions between the catalyst and the underlayer metal. The CNT via test structure has been designed and fabricated to make current–voltage measurements on single CNTs using a nanomanipulator under scanning electron microscopy (SEM) imaging. By analyzing the dependence of measured resistance on CNT diameter, the CNT–metal contact resistance can be extracted. The contact resistances between as-grown CNTs and different underlayer metals are determined. Relationships between contact resistances and various combinations of catalysts and underlayer metals are investigated.

(Some figures in this article are in colour only in the electronic version)

1. Introduction

Vertically aligned carbon nanotubes (CNTs) directly grown on metal electrode underlayers are promising materials in applications such as on-chip interconnects, nanoelectrode arrays, nanoelectromechanical devices and field emission devices [1–3]. For such applications, both the electrical properties and geometrical control (alignment, diameter, length, etc) are critical factors in device fabrication and performance. Thus it is necessary to compare the growth of CNTs on different underlayer metals for fabricating devices compatible with existing complementary metal oxide semiconductor (CMOS) technology. Although several metals have been studied [4–6], optimizing growth to obtain vertically aligned CNTs (as well as carbon nanofibers (CNFs)) with well-controlled geometry and low resistance remains a challenge.

Aside from compatibility with CMOS process technology, the underlayer metal must not react with the catalyst (e.g. Ni, Fe, Co) to form alloys at CNT growth temperatures, which may poison the catalyst in the reaction. Also, the underlayer metal must form good electrical contact with the as-grown CNT, with low contact resistance. Finally, the underlayer metal must have good adhesion to the catalyst as well as the silicon substrate, while maintaining sufficient wettability with the liquid phase of the catalyst, so that the catalyst film can easily form uniform and discrete nanoparticles during the pre-growth thermal annealing process. In this paper, Ti, Cr and Al are chosen as the underlayer metals to study the growth behaviors of vertically aligned CNTs, together with the two most common catalysts, Ni and Fe. A critical thickness of catalyst film is determined in each case. The average diameter, diameter distribution and density of CNTs vary with the metal underlayer. The very different growth rates of CNTs are also obtained for different combinations of catalysts and underlayer metals. These observations are explained in terms of interactions between the catalyst and underlayer metal. The nanostructures of as-grown CNTs from

[3] Author to whom any correspondence should be addressed.

each metal–catalyst combination are also characterized using high-resolution transmission electron microscopy (HRTEM).

Four-point-probe measurements have been widely adopted to extract bulk and contact resistances for horizontal one-dimensional nanostructures [7, 8]. However, it is challenging to fabricate the corresponding four-point test structures for vertical nanostructures such as vias due to the complex 3D nature of the electrode–via system (in CMOS integrated circuits, a via is a small opening in an insulating oxide layer that allows a conductive connection between adjacent layers). Therefore, finding an alternative way to extract contact resistance in a via structure is critically needed. Measured electrical characteristics of CNT vias have been reported [9, 10], but few articles focus on the differentiation of contact resistances from the overall via resistances. In our previous work [11], the CNT via test structure has been designed and fabricated to make current–voltage measurements on single CNTs using the atomic force microscope (AFM) current-sensing technique. By analyzing the dependence of measured resistance on CNT diameter, the metal–CNT contact resistance can be extracted [11]. Due to difficulties in locating a single CNT cross section under AFM imaging and weak contact force between AFM probe tip and CNT resulting in large contact resistance, a nanomanipulator system in the SEM chamber has been used for I–V measurements. The nanomanipulator tip with 20 nm in diameter can directly engage on the CNT cross section under SEM imaging. With the prototype vertically aligned CNT via structures, the contact resistances between the single CNTs and several different underlayer metals are determined. Chemical bonding at the interface between CNT and underlayer metal is investigated and the observed metal oxide leads to high contact resistance as confirmed by electrical measurement. The CNT growth parameters are correlated with the nanostructure and measured contact resistance, yielding a useful scheme for characterizing the growth process.

2. Experimental details

There are two general approaches to prepare the catalyst for CNT growth. One is to deposit a catalyst layer and then transform it into nanoparticles by heating and/or plasma etching before introducing hydrocarbon source. The other is to spin-coat the premade nanoparticles in solution onto the substrate. The latter can result in desirable diameter distribution and density by controlling uniformity and concentration (and optimizing the spin condition) of the nanoparticle solution, respectively. However, the nanoparticle solution can bring organic contamination into the process and is not CMOS-compatible. The former method is compatible with the current CMOS process and the catalyst can be patterned. But the density and diameter distributions of the CNT are not easily controlled, which depend on the pretreatment condition and the underlayer material. In turn, the pretreatment condition and the properties of the underlayer material also affect the growth and CNT quality. The optimal pretreatment condition has been obtained with thermal annealing for 3–5 min at 600 °C under ∼2 mbar NH_3 atmosphere for various catalysts and underlayer metals.

In this study the underlayer metal and catalyst thin films are deposited in sequence on an Si substrate in the same electron-beam evaporation system. Films of Ti, Cr or Al (30 or 80 nm) are deposited on Si wafers using e-beam evaporation, followed by a catalyst film (Ni or Fe: 5, 10, or 20 nm) deposition in the same chamber, without breaking vacuum. The vertically aligned CNTs are then grown using a DC plasma-enhanced chemical vapor deposition (PECVD) system consisting of a resistively heated graphite substrate stage with controllable temperature. Typically, the catalyst film is thermally annealed in ammonia at 600 °C for 3 min to form particles, prior to CNT growth at 750 °C. All growths are carried out at 7 Torr in a 4:1 mixture of NH_3:C_2H_2 for 15 min. The plasma power is set at 210 W with an applied voltage of 530 V. The morphology and nanostructure of as-grown CNT samples are analyzed using scanning electron microscopy (SEM, Hitachi S-4800), high-resolution transmission electron microscopy (HRTEM, Hitachi HD 2300-A), and Raman spectroscopy (Jobin Yvon/Labram HR800). The thermally annealed catalyst samples are characterized by SEM and atomic force microscopy (AFM, Veeco Dimension 3100). X-ray photoelectron spectroscopy (XPS, SSI S-Probe) is used to determine the composition and core-state chemical shifts of the different metal species during the process.

In order to carry out resistance measurements, a CNT via test structure is fabricated. The fabrication process has been described in detail elsewhere [12]. To summarize, the CNT arrays grown on metal underlayers are first embedded in tetraethylorthosilicate (TEOS) oxide to achieve structural rigidity and electrical isolation. The sample is then polished using a chemical–mechanical planarization (CMP) process to expose the CNTs for direct electrical probing. The top patterned 50 nm thick Pt electrodes are finally deposited on the sample with 5 nm Ti thin film as the interlayer. The contact resistance between single CNT and underlayer metal is extracted using a nanomanipulator system in the SEM chamber.

3. Results and discussion

First, we study the effect of catalyst film thickness on CNT growth. Unlike growth on an SiO_2 substrate, which results in high-density CNTs using Fe or Ni catalyst films 5 nm or thinner (figure 1(d)), the same catalyst on Ti or Cr underlayer has a critical thickness of 10 nm (figures 1(a)–(c)). When the catalyst thickness is below 10 nm, continual and high-density CNT growth is not observed. Figure 1(a) (top frame) shows a SEM image of a 5 nm Ni film deposited on Ti. The same sample reveals few particles found on the metal underlayer after annealing (figure 1(a) middle and bottom frames). Apparently, for such a film thickness, Ni evaporates from the Ti substrate. This conclusion is confirmed by XPS results. For a typical sample with 5 nm of Ni on 30 nm of Ti, after annealing at 600 °C the Ni:Ti atomic ratio changes to 0.03 from 36.5 before annealing. Metallic Ni or Fe can form an interfacial bond with the surface oxygen atoms of the oxide, which increases the catalyst film adhesion [13] and decreases the mobility of individual metal atoms, whereas

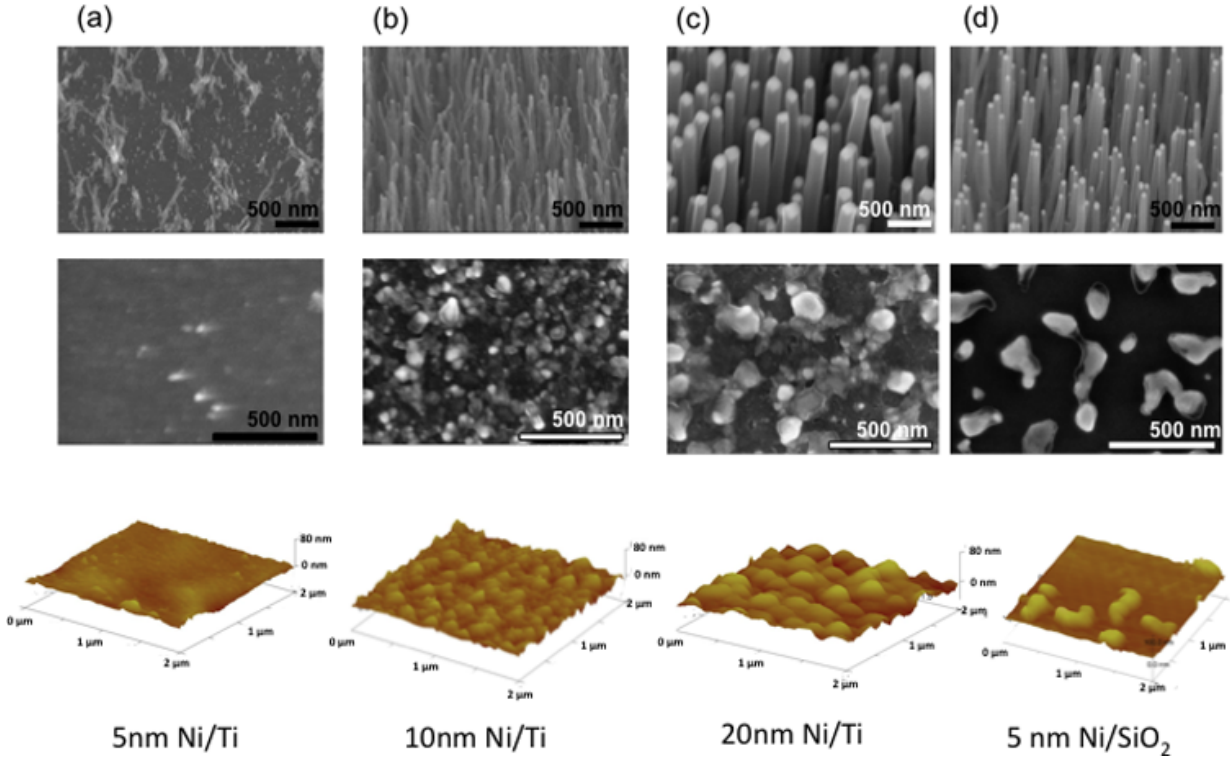

Figure 1. Effect of catalyst film thickness on CNT growth on 80 nm Ti underlayer. SEM images of CNTs grown (top frames), SEM image (middle frames) and AFM images (bottom frames) of catalyst particles formed by 600 °C thermal annealing. (a) 5 nm Ni/80 nm Ti, (b) 10 nm Ni/80 nm Ti, (c) 20 nm Ni/80 nm Ti, (d) 5 nm Ni/30 nm SiO_2.

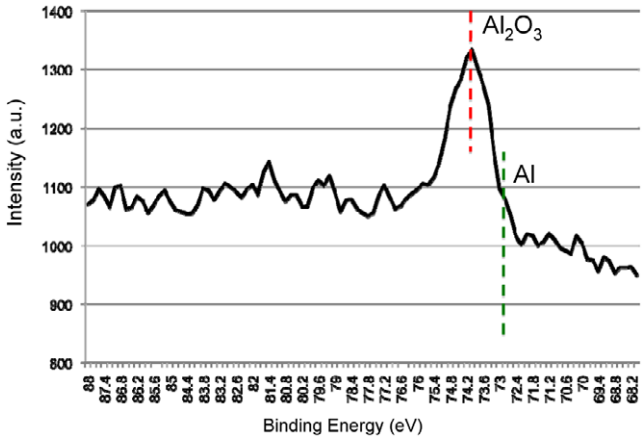

Figure 2. XPS spectrum of Al 2p in 5 nm Fe/10 nm Al/30 nm Ti/Si sample.

there is no such strong interaction between Ni and the Ti underlayer. In addition, due to a smaller wetting angle between Ti and liquid Ni [14, 15], compared to that between SiO_2 and liquid Ni [14, 15], Ni has a tendency to preserve the thin film morphology on Ti during thermal annealing, which in turn accelerates the evaporation of Ni. Thus a thick Ni film is needed to form catalyst particles for optimal CNT growth. The same results have been observed for Ni on Cr, and Fe on Ti or Cr.

When a thin Al buffer layer is introduced between the Fe catalyst film and Ti underlayer, no critical thickness is observed. High-density and uniform CNT diameters are obtained with a 10 nm Al buffer layer underneath a 5 nm Fe catalyst film. However, XPS results shown in figure 2 indicate that, in fact, the Al layer had been oxidized even before the CNT growth process. The resulting alumina is bonded strongly to the underlayer Fe, even stronger than SiO_2 [16], and alumina has as large a wetting angle with Fe [14] as that of SiO_2. However, alumina is an insulator, resulting in a virtual open circuit between the top and bottom electrodes during resistance measurements (see table 1). Thus we are unable to determine the contact resistance between CNT and underlayer metal for this test structure. The same result is obtained for the Ni/Al/Ti combination, strongly suggesting that Al is unsuitable as an underlayer metal for via interconnect applications. A summary of results for six different catalyst/underlayer combinations is shown in table 1.

A strong correlation is found between the catalyst film thickness and the CNT density and diameter. In most cases, thicker catalyst film results in larger average CNT diameter and lower-density growth (table 1). In addition, various growth rates are observed. In particular, Fe shows an extremely low growth rate on Ti and Cr. It was reported that the growth rate of CNTs increased with decreasing Ni particle size on an Si substrate [17], which is not observed in this study with Ni on Ti or Cr. Our results suggest that the CNT growth behaviors depend not only on the catalyst itself but also on the underlayer material. Further studies are needed to elucidate this complex dependence.

The nanostructures of as-grown CNTs are also investigated using HRTEM (figure 3). Fe-catalyzed CNTs have

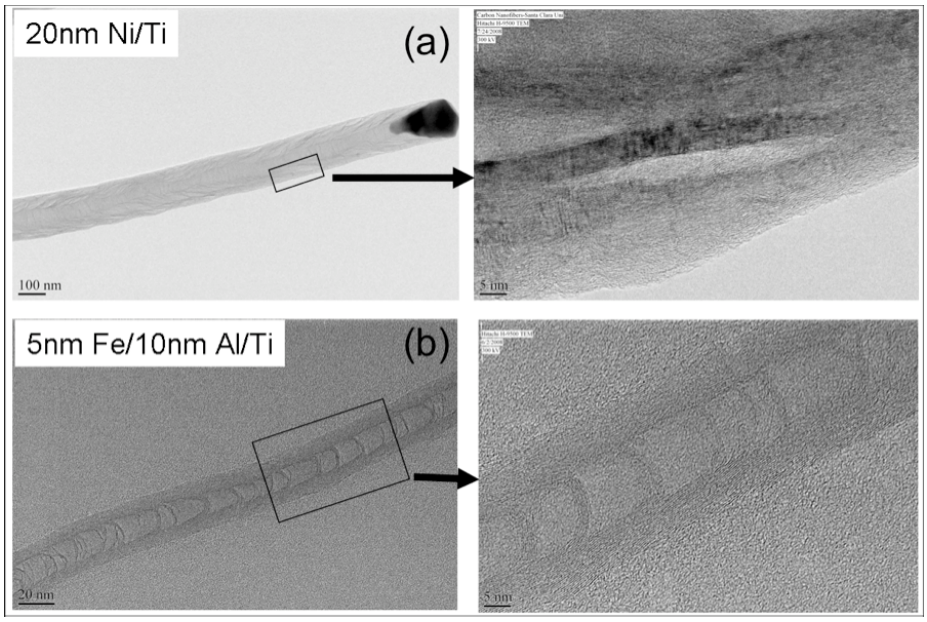

Figure 3. TEM images of CNTs grown with (a) 20 nm Ni/Ti underlayer and (b) 5 nm Fe/10 nm Al/Ti underlayer.

Table 1. Length, average diameter, and density of CNTs grown with different combinations of catalysts and metal underlayers. Measured contact resistance is also given wherever applicable, except the 10 nm Ni/Ti, 10 nm Fe/Ti and 10 nm Fe/Cr samples, which has the same catalyst/underlayer combination as the next one.

Catalyst/metal	Length (μm/15 min)	Av. dia. (nm)	Density (#/μm^2)	Contact resistance (kΩ)
10 nm Ni/Ti	5.1	40 ± 20	60	—
20 nm Ni/Ti	5.1	120 ± 50	30	4.2
10 nm Ni/ 10 nm Al/Ti	3.46	40 ± 30	65	Indeterminate due to Al_2O_3 formed
20 nm Ni/Cr	4.74	120 ± 50	35	5.0
5 nm Fe/ 10 nm Al/Ti	4.74	40 ± 10	75	Indeterminate due to Al_2O_3 formed
10 nm Fe/Cr	1.36	60 ± 20	46	—
20 nm Fe/Cr	1.41	80 ± 20	38	3.8
10 nm Fe/Ti	1.42	60 ± 30	50	—
20 nm Fe/Ti	1.79	60 ± 40	70	1.8
5 nm Ni/SiO_2	4.74	50 ± 30	60	N/A

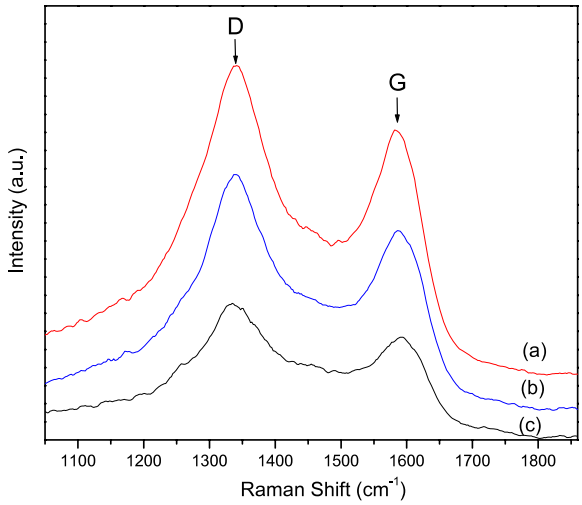

Figure 4. Raman spectra of CNTs grown with 20 nm Ni/80 nm Cr (curve (a)), 20 nm Ni/80 nm Ti (curve (b)) and 5 nm Ni/30 nm SiO_2 (curve (c)), showing the D and G band peaks in each.

an orderly structure with straight and concentric cylindrical graphene walls, while Ni catalysts yield stacked-cup structures, which resemble those in CNFs [5]. The two-dimensional disordered morphology of graphitic layers in CNF underscores the key difference between CNT and CNF [2, 4, 5]. While the nanofiber exhibits a stacked-cone morphology defined by a non-zero cone angle, an ideal nanotube has a cone angle of zero degrees. Thus the interior of a CNF is no longer hollow as in CNT. Under an electron microscope, the main characteristic distinguishing CNF from CNT is the presence of cone-shaped stacked graphene sheets in a CNF. The TEM images reveal that the quality of Ni-catalyzed CNTs or CNFs is not strongly dependent on catalyst film thickness and the choice of underlayer metal. In this case, the nanostructures are determined largely by the carbon solubility in Ni and diffusion of Ni and carbon source (C_2H_2) during growth, and not affected much by the Ni particle size and metal underlayer. The quality of Ni-catalyzed CNT/CNF samples with different underlayers is also examined by Raman spectroscopy. Figure 4 shows the Raman spectra of CNTs grown with 20 nm Ni/Ti, 20 nm Ni/Cr and 5 nm Ni/SiO_2. The Raman spectra of as-prepared samples of Ni/Ti, Ni/Cr and Ni/SiO_2 show similar features with D band and G band peaks at 1340 and 1585 cm^{-1}, respectively. The quality of CNTs samples can be inferred from the intensity ratio between D band (disorder) to G band (graphite) (I_D/I_G). The I_D/I_G values of 20 nm Ni/Ti, 20 nm Ni/Cr and 5 nm Ni/SiO_2 are 1.22, 1.20 and 1.23, respectively, further revealing

that the quality of CNTs is independent of the Ni thickness and underlayer metals.

The development of conductive AFM and nanomanipulators in SEM chambers makes it possible to carry out current–voltage (I–V) measurement directly on individual nanostructures. The surface topographic image obtained for a CNT via sample allows us to systematically locate single CNTs for I–V measurements. The resistance (R_{Total}) obtained from the measured I–V curves consists of the CNT bulk resistance (R_{CNT}) in series with the total contact resistance (R_{C}):

$$R_{\text{Total}} = R_{\text{C}} + R_{\text{CNT}}, \tag{1}$$

where R_{C} represents the sum of CNT–metal and probe tip–CNT contact resistances. The contact resistance between the probe tip and the CNT is dependent on the pressure applied on the tip, and can be minimized empirically. The contact resistance between the nanomanipulator tungsten probe and CNT is lower than that of the AFM tip–CNT, as will be revealed below. When the CNF length L_{CNT} is much larger than the electron mean free path λ_{CNT}, R_{CNT} can be expressed as

$$R_{\text{CNT}} = \frac{4\rho L_{\text{CNT}}}{\pi D_{\text{CNT}}^2}, \tag{2}$$

where ρ is the CNT resistivity and D_{CNT} the diameter. If we assume the contact resistance is constant and independent of D_{CNT} [11], R_{Total} in equation (1) becomes a linear function of $1/(D_{\text{CNT}})^2$. Plotting R_{Total} versus $1/(D_{\text{CNT}})^2$ and extrapolating to zero yields R_{C} [11]. For example, the extracted contact resistance of a CNT via test structure on a Ti underlayer with a 20 nm Ni catalyst film, obtained from AFM measurements, is 6.4 kΩ with an error bar of about 400 Ω, and the resulting CNT average resistivity is 7.3×10^{-4} Ω cm. A lower contact resistance of 4.2 kΩ is obtained for the same catalyst–underlayer combination if a nanomanipulator probe is used. The difference of 2.2 kΩ between the two measurement techniques is most likely due to the higher contact resistance between the AFM probe tip and CNT compared to that between the nanomanipulator probe tip and CNT. Using this method, the contact resistances between CNTs grown with catalyst Ni or Fe and various underlayer metals are extracted and given in table 1.

The nature of the interface between CNT and underlayer metal is critical to the contact property between them. The formation of an insulating or semiconducting oxide or carbide is harmful to achieving low contact resistance between CNT and underlayer metal, as demonstrated earlier in the use of an Al buffer layer. The chemical state evolution of the underlayer metal is investigated using XPS. We find that both the Ti and Cr underlayers have been oxidized after thermal annealing and CNT growth. Figure 5(a) shows the XPS spectra of Cr 2p in a 20 nm Ni on 80 nm Cr sample as-prepared, after 600 °C thermal annealing for 3 min, and after 30 s CNT growth. Cr oxide peak appears after the annealing and stays even after CNT growth. The same phenomenon is observed in Ti underlayer samples shown in figure 5(b). The oxidation occurs either during the growth process due to residual oxygen in the PECVD chamber or after exposure to air. The average

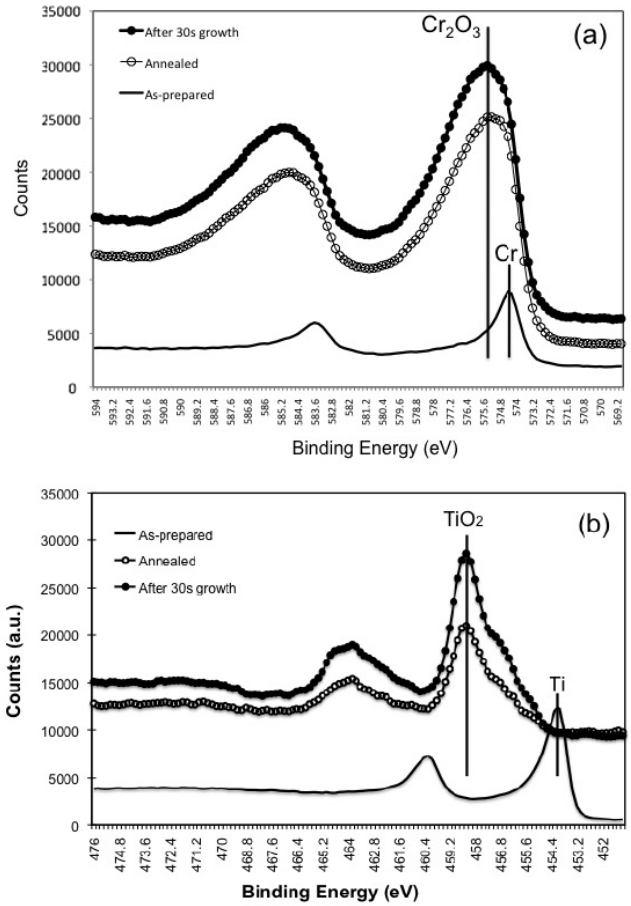

Figure 5. XPS spectra of (a) Cr 2p in 20 nm Ni/80 nm Cr, (b) Ti 2p in 20 nm Ni/80 nm Ti samples under different growth conditions.

contact resistance R_{C} extracted from measured single CNT resistances versus varying diameters ranges between 1.8 and 5.0 kΩ. Unlike low resistance for metal–metal contacts, R_{C} values obtained here are generally larger than the bulk CNT resistance (with average resistivity of 7.3×10^{-4} Ω cm) with similar dimensions. The contact resistance therefore dominates the electrical characteristics of carbon nanostructures in via interconnects. The metal oxide formation between CNT and underlayer metal is one of the major causes of large contact resistance.

4. Conclusions

The growth behaviors of vertically aligned CNTs grown on different metal underlayers have been investigated. A critical thickness (∼10 nm) of Fe or Ni catalyst film is needed to grow CNTs on various underlayer metals. The average diameter and density of CNTs exhibit a strong correlation with the choice of catalyst–underlayer combination. XPS analysis of the interface between catalyst and underlayer metal reveals metal oxide formation, which leads to large contact resistance between CNT and underlayer metal. Further process improvement to control underlayer metal oxidation is needed to reduce contact resistance.

Acknowledgments

This work is supported by the United States Army Space and Missile Defense Command (SMDC) and carries Distribution Statement A, approved for public release, distribution unlimited.

References

[1] Awano Y 2006 *IEICE Trans. Electron.* **E89–C** 1499
[2] Li J, Ng H T, Cassell A, Fan W, Chen H, Ye Q, Koehne J, Han J and Meyyappan M 2003 *Nano Lett.* **3** 597
[3] Teo K B K *et al* 2004 *IEE Proc. Circuits, Devices Syst.* **151** 443
[4] Ng H T, Chen B, Koehne J E, Cassell A M, Li J, Han J and Meyyappan M 2003 *J. Phys. Chem.* B **107** 8484
[5] Cassell A M, Ye Q, Cruden B A, Li J, Sarrazin P C, Ng H T, Han J and Meyyappan M 2004 *Nanotechnology* **15** 9
[6] Kabir M S, Morjan R E, Nerushev O A, Lundgren P, Bengtsson S, Enokson P and Campbell E E B 2005 *Nanotechnology* **16** 458
[7] Bachtold A, Henny M, Terrier C, Strunk C, Schonenberger C, Salvetat J P, Bonard J M and Forro L 1998 *Appl. Phys. Lett.* **73** 274–6
[8] Walton A S, Allen C S, Critchley K, Gorzny M L, McKendry J E, Brydson R M D, Hickey B J and Evans S D 2007 *Nanotechnology* **18** 065204
[9] Kawabata A *et al* 2008 *Proc. IEEE 2008 Int. Interconnect Technology Conf.* pp 237–9
[10] Coiffic J C, Fayolle M, Le Poche H, Maitrejean S and Olivier S 2008 *Proc. IEEE 2008 Int. Interconnect Tech. Conf.* pp 153–5
[11] Wu W, Krishnan S, Yamada T, Sun X H, Wu R, Li K and Yang C Y 2009 *Appl. Phys. Lett.* **94** 163113
[12] Wu W, Krishnan S, Li K, Sun X H, Wu R, Yamada T and Yang C Y 2009 *Proc. IEEE 2009 Int. Conf. Microelectronics Test Structures* pp 27–30
[13] Diebold U, Pan J-M and Madey T E 1995 *Surf. Sci.* **331–333** 845
[14] Asthana R and Sobczak N 2000 *JOM-e* **52** 1
[15] de Gennes P G 1985 *Rev. Mod. Phys.* **57** 827
[16] Mattevi C *et al* 2008 *J. Phys. Chem.* C **112** 12207
[17] Choi Y C, Shin Y M, Lee Y H, Lee B S, Park G S, Choi W B, Lee N S and Kim J M 2000 *Appl. Phys. Lett.* **78** 2367